

# A Model for Impulsive Power-Line Radio Disturbance Due to Gap-Type Discharges

PAUL H. MOOSE, MEMBER, IEEE, AND JOHN M. O'DWYER, MEMBER, IEEE

**Abstract**—Electromagnetic disturbance from power lines is one of the main sources of man-made noise affecting communications in the high-frequency radio band. Most radio disturbances generated by power lines are of two types: gap-type noise caused by electric discharges across line hardware, and corona noise caused by the partial breakdown of the air due to the high electric fields around transmission-line conductors. While the physical mechanisms of these noise types have been investigated in detail, these studies have not yet been used to develop noise models for the evaluation of communication-system performance. This paper presents a mathematical model that allows the fundamental mechanisms of gap-type noise to be simulated. With this model, the effect of gap-type noise processes on various high-frequency communication systems can be determined by direct computation as well as by experimental observation. The mathematical model was used to derive an expression for the demodulated power spectral density (PSD) compared with field observations.

**Key Words**—Man-made noise, gap-type noise, radio disturbance, power lines.

**Index Code**—B4e, B3e.

## I. INTRODUCTION

THIS study is part of an ongoing effort by the Naval Postgraduate School to catalog radio-disturbance sources at fixed high-frequency (2–30 MHz) radio-receiver sites [1]. A significant amount of qualitative data has been obtained which supports the conclusion that power-line noise is a major source of man-made radio noise in the high-frequency band [2]. A second conclusion is that, in any given disturbance scenario, there is usually one identifiable dominant source of disturbance [3]. Since gap-noise is one of the major types of disturbance from power lines, it was frequently observed as the primary disturbance.

At least two mechanisms have been found by which a gap discharge process can occur on a power line. The resistance in the line insulators can be degraded, allowing current to flow through the insulator base, thereby creating a potential gradient across any gaps or defects in the insulator mounting hardware. A second way in which a potential can be created across an air gap is by an electrostatic coupling of the line potential to isolated hardware on the pole. In both cases, the potential across the gap is discharged by the voltage breakdown of the gap and the resulting rapid current flow or spark. This process generates an RF noise impulse with spectral

components extending into the hundreds of megahertz. During a single discharge, the potential across the gap is temporarily diminished. However, while the fundamental 60-Hz waveform is still above, or below, an absolute threshold voltage, the process can occur again. The spark will discharge across the gap repeatedly until the alternating current waveform drops below the breakdown threshold potential [4], [5].

The spark discharge and recharging of the gap potential indicates that this type of process is regenerative and can be modeled as a renewal process where the renewal points are associated with the sparks. One feature of gap noise that complicates the modeling is the 120-Hz on-off-on modulation imposed on the renewal points by the alternating current waveform. One way to account for this effect is to consider the turn-on time as another renewal process driving the spark discharge process. This type of model is known as a branching renewal process [6].

The noise processes that were used to develop this model were short-term stationary in that the statistics of the process were essentially constant over the observation interval. Stationarity was further assured by distributing the start of the data records uniformly over one cycle of the fundamental power-line waveform. Not all sources of power-line noise are stationary, even over a short observation interval. Physical effects such as wind, solar heating, and varying line loads can act to make certain types of power-line noise highly variable from one observation to the next. Although these types of noise were observed during data collection, the data used to develop and test the model were taken from noise sources that were essentially stationary for the length of the 10-min data records.

## II. INSTRUMENTATION

Two instrumentation configurations were employed to provide data on the detailed time- and frequency-domain properties of HF radio noise. They are switch selectable and are both shown in Fig. 1. Either a fixed HF long-wire antenna or a whip antenna mounted on a mobile van provided the  $E$ -field RF input signals to the instruments.

In Fig. 1, a Hewlett-Packard 141T Spectrum Analyzer is used as the scanning analyzer to drive a Develco 7200B three-axis display. The spectrum analyzer can be tuned to any desired frequency in the HF band. Its scan rate, scan width, IF bandwidth, IF gain, RF attenuation, and other controls can be adjusted to best capture the noise source under observation.

An alternate and complementary measurement system can be selected to examine the narrow-band properties of HF noise. An HF receiver is used as an amplifier/translator and tuned to

Manuscript received December 9, 1985; revised March 24, 1986.

P. H. Moose is with the Department of Electrical and Computer Engineering, Naval Postgraduate School, Monterey, CA 93943. (408) 646-2838.

J. M. O'Dwyer is with Naval Security Group Headquarters, Washington, DC 20390-5210. (202) 282-0880.

IEEE Log Number 8610578.

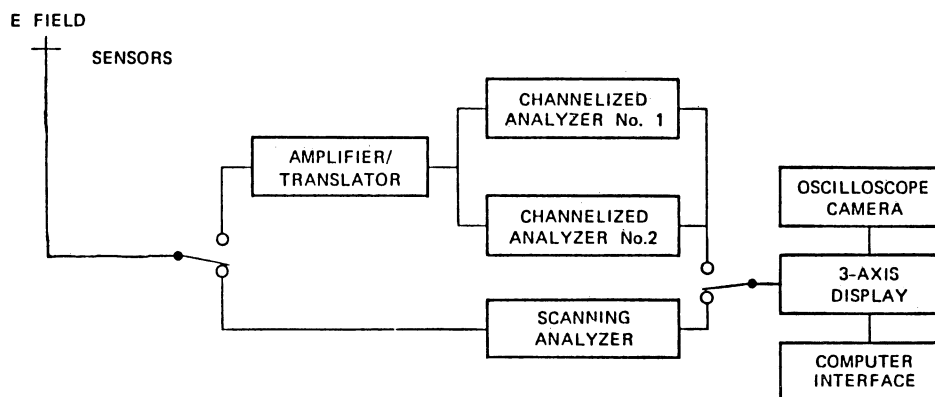


Fig. 1. Simplified block diagram of measurement system.

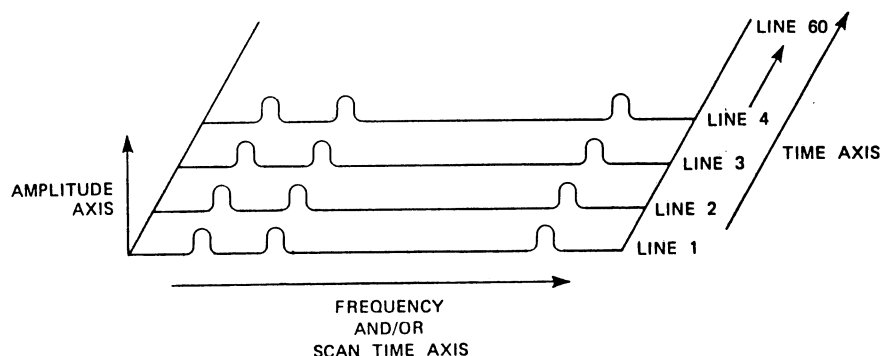


Fig. 2. Diagram of data format.

a frequency where the noise is present. The demodulated audio output is then directed to a Wavetek (Nicolet) UA500A channelized analyzer which subdivides the audio-output spectrum into 500 frequency segments. When the full audio-output bandwidth of 5 kHz is examined, the UA500A provides a frequency resolution of 10 Hz per segment. The Wavetek analyzer can provide individual transforms or average a selected number of successive transforms. The transforms (either individual or averaged) are then presented on the three-axis display.

The three-axis display provides a continuous moving real-time visual representation of the analog output from the spectrum analyzers or narrow-band receiver audio output. The receiver or analyzer output analog data are digitized in the display and stored in a semiconductor memory. The data in the memory are formatted and shown on a CRT in a convenient frequency-amplitude-time (three-axis) format. The three-axis presentation can be frozen at any desired time and photographed with a standard oscilloscope camera.

Fig. 2 illustrates the procedure used to make the three-axis presentation. The analog input is divided into 512 equally spaced data points along the scan time axis. The signal amplitude at each data point is represented by an 8-bit word. When a scan is completed, its data are stored in memory. Line 1 in the view moves to line 2, and the new scan appears as line 1. Subsequent scans move earlier data, line by line, upwards along the time axis to create a rising-raster-type display. When the memory is full (64 scans), each new scan is entered into the bottom line, and the oldest data at the top line are discarded. When the spectrum analyzer output is being displayed, the

resulting animated view provides a visual picture of noise and signals within a chosen block of frequencies. If the receiver audio output is being observed, the display is a stacked series of consecutive time records.

### III. OBSERVED TIME-DOMAIN CHARACTERISTICS

The gap-noise sources for this study were observed on utility distribution lines in the vicinity of the Naval Postgraduate School and were chosen to illustrate parameters of the noise model. Fig. 3 is a typical time-domain observation of a gap discharge process observed at 3 MHz and envelope demodulated with a 10-kHz Gaussian bandpass filter. The important characteristics to note are the following.

- The process has an on-off-on modulation at a 120-Hz rate related to 60-Hz waveform of the power line.
- The pulse groups that result from the modulation have a variable number of impulses occurring in each group and random interarrival times between pulses in a group.

In the first pulse group, nine pulses occur with varying amplitudes and interpulse arrival times. In the second pulse group starting approximately 8.33 ms later, eight pulses occur, again with varying amplitudes and interarrival times. One group of pulses is associated with either the positive or negative polarity of the line voltage waveform and the other group with the opposite polarity. Identification of the polarity is impossible without physically locating the source.

The average amplitude of the impulses will be one of the parameters for the model. An estimate of this parameter can be obtained from the above presentation. It is important to note

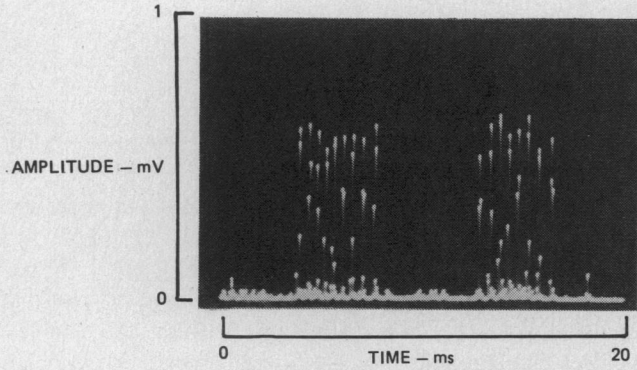


Fig. 3. Envelope of demodulated gap-noise disturbance recorded in the time-domain: 10-MHz center frequency, 10-kHz IF frequency.

that, for this highly impulsive type of noise, the actual observed amplitude is a function of the shape and width of the effective bandpass filter and the detector characteristics.

In order to better characterize the interpulse arrival times, which will be used to determine two additional model parameters, the rising-raster capability described in the instrumentation section was used to generate the display of a different gap-noise source which is shown in Fig. 4. In this picture, the amplitude of each individual record was normalized to one so that the only remaining information is the time of impulse arrivals for 28 time records. The amplitude data are suppressed in this type of presentation. The time base of the display was intentionally synchronized to the power line to facilitate taking data, and accounts for the regularity of the pulse groups from observation to observation. In this view, the interarrival times for 56 pulse groups can be determined along with the number of pulses in each of the 56 successive pulse groups. The average number of pulses per group will also be used as an estimate of a parameter for the model.

Fig. 5 is a histogram of the distribution of the interarrival times between the observed impulses for the same noise process shown in Fig. 4. To use these data to generate parameters for a noise model, the histogram will be fitted to a continuous density function. The gamma density function [7]

$$f(t) = \lambda(\lambda t)^{r-1} e^{-(\lambda t)} / (r-1)!, \quad t > 0 \quad (1)$$

was chosen because it showed a close fit to the data and its characteristic function, which will be used in later derivations, was particularly simple. The characteristic function of the gamma density is

$$\phi(j\omega) = (1 - j\omega\lambda)^{-r}. \quad (2)$$

The  $r$  and  $\lambda$  parameters are simply interpreted in terms of an underlying Poisson process as the time to the  $r$ th point of a Poisson process of intensity  $\lambda$ . If  $\mu$  is the random variable assigned to the observed interarrival times, then the unbiased estimate of the mean of  $\mu$  is

$$\text{est}(\bar{\mu}) = (1/N) \sum_{i=1}^N \mu_i \quad (3)$$

and the unbiased estimate of the variance is

$$\text{est}(\sigma_\mu^2) = \left\{ \sum_{i=1}^N \mu_i^2 - N \cdot \text{est}(\bar{\mu})^2 \right\} / (N-1). \quad (4)$$

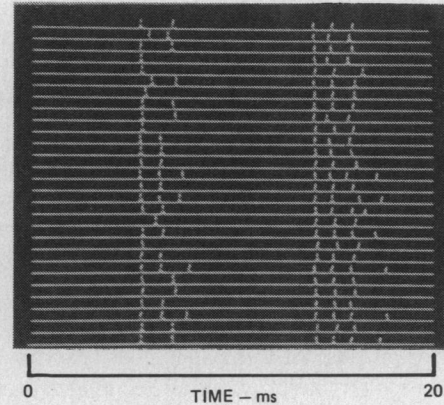


Fig. 4. Multiple scans of gap-noise disturbance. Scan start time is synchronized to the power line, and amplitude information is suppressed to show pulse timing structure: 7.1-MHz center frequency, 10-kHz IF frequency.

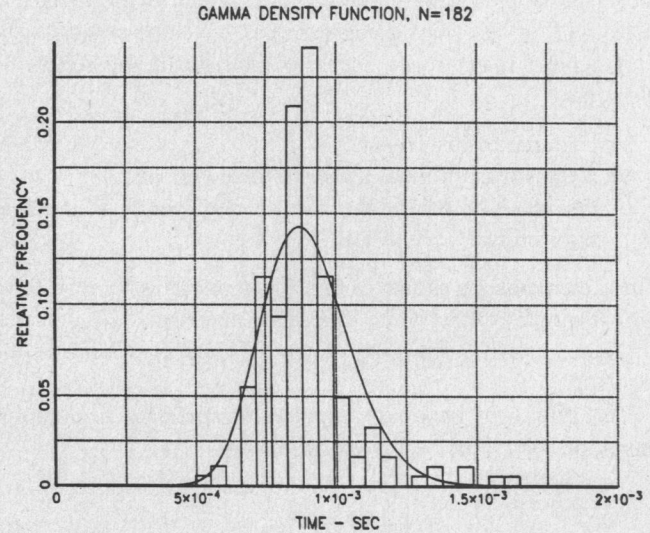


Fig. 5. Histogram of interpulse arrival times from one gap-noise source. Gamma density function is fitted to data using method of moments.

The unknown parameters of the desired gamma density function are estimated using the method of moments [8] according to

$$r = \text{est}(\bar{\mu})^2 / \text{est}(\sigma_\mu^2)$$

and

$$\lambda = \text{est}(\bar{\mu}) / \text{est}(\sigma_\mu^2). \quad (5)$$

Fig. 5 also shows the gamma density function used to approximate the interarrival time histogram using this approach.

In summary, the inputs to the model based on time-domain data are:

- a) an estimate of the average amplitude of all observed pulses;
- b) an estimate of the average number of pulses per group;
- c) an estimate of the mean of the interarrival time of the pulses; and
- d) an estimate of the variance of the interarrival time between pulses.

The average amplitude of pulses from different gap-noise sources is highly variable, ranging from the instrumentation noise floor to higher than any observable signal in the high-frequency band. The average number of pulses per group has been observed to vary from 1 to greater than 20. The mean of the interarrival times ranges from 0.1 to 1 ms, and the coefficient of variation (standard deviation divided by the mean) of the interarrival times has ranged from approximately 0.1 to 0.3 for the gap-noise processes we have observed.

#### IV. IMPULSIVE NOISE AND RECEIVER MODEL

The major purpose of this paper is to describe a relatively simple noise model that provides an accurate representation of a gap-type noise process. The noise process at the receiver will be modeled as the sum of a high-density (in time) low-amplitude Gaussian component and a low-density high-amplitude impulsive term. In order to provide a framework for the discussion, a general disturbance scenario for impulsive noise will be described using complex envelope notation [9].

A typical interference scenario consists of the following elements:

- a source of disturbance;
- a transmission medium to the receiver; and
- the receiver where the disturbance manifests itself as interference.

These elements are shown in Fig. 6 where  $a(t)$  is the impulsive disturbance,  $w(t)$  is white Gaussian noise and  $H(\omega)$  is the combined transfer function of the RF and IF filters of the receiver.

The source of bandpass impulses is specified in complex envelope form [10] by the equation

$$a(t) = \sum_{i=1}^{N(t)} a_i e^{j\theta_i} \delta(t - t_i) \quad (6)$$

where  $a_i$  is the amplitude of the  $i$ th pulse and  $N(t)$  is the unit counting process that generates the  $t_i$ 's.  $\theta_i$  is the phase of the impulse arrival time at the receiver with respect to the reference frequency  $\omega_0$ . It can be assumed that  $\theta_i$  is uniformly distributed over 0 to  $2\pi$  when the  $t_i$ 's have a random interarrival distribution and  $\omega_0$  is much greater than the inverse of the interarrival times [11], [12]. With this representation, the impulsive interference source is described by the probability density function of each  $a_i$  and the impulse arrival times generated by  $N(t)$ .

In order to physically justify a filtered impulse model, the impulse duration must be small compared to the inverse bandwidth of the receiver filter. This condition is easily met in the case of gap discharges. Laboratory analysis of temporal characteristics of gap discharges for various geometries shows that the impulse durations range from 10 to hundreds of nanoseconds [13]. Therefore, for filter bandwidths up to 1 MHz, the output noise process will only be a function of the incident time of the impulse and the filter response, not the waveform of the impulse.

The Gaussian component  $w(t)$  in Fig. 6 is due to the combination of: a) the thermal noise in the receiver; and b) the

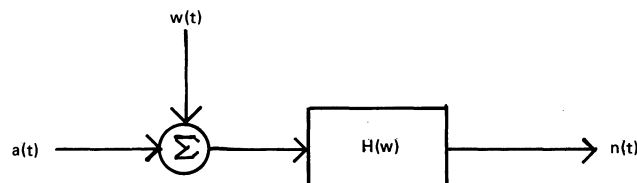


Fig. 6. Block diagram of interference scenario. Complex envelope notation is used.

combined sum of many low-level atmospheric or man-made impulsive sources. The distinction between the low-level impulses that combine to create Gaussian noise and impulsive noise is that the receiver responses overlap for the high-density low-amplitude case satisfying the condition for the Central Limit Theorem. For the impulsive noise, the receiver response to each impulse is discernible such that the probability of more than one or two pulses overlapping is negligible.

The input to the receiver is then given by

$$n(t) = g(t) + h(t) * \sum_{i=1}^{N(t)} a_i e^{j\theta_i} \delta(t - t_i) \quad (7a)$$

where

$$h(t) = h_i(t) + jh_q(t) \quad (7b)$$

and  $h_i(t)$  and  $h_q(t)$  are the in-phase and quadrature components of the filter impulse response. If  $B$  is the effective white-noise bandwidth of  $H(\omega)$ , then

$$g(t) = (h(t)/2) * w(t) \quad (8)$$

where  $g(t)$  is a zero mean Gaussian process with a variance of  $N_0 B/2$  in the in-phase and quadrature terms.

The specification of the statistics of  $N(t)$ , the counting process that drives the model, is crucial to obtaining an accurate representation of the physical noise process. Based on the electrical characteristics of a gap discharge detailed in the previous section, the following assumptions were made.

- A primary series of event times exists spaced at an interval  $T_0/2$ .  $T_0$  is the fundamental period of the power-line voltage waveform. The distribution of the time to the first primary event is uniform over  $T_0/2$ .
- A subsidiary process commences at the primary event times, i.e.,  $T_0/2, T_0, 3T_0/2, \dots$ , etc. The subsidiary process is a renewal process that continues for  $N$  renewals.
- The interarrival times to the first and subsequent points of the subsidiary renewal process are all independent and identically distributed.
- At each point in the subsidiary process, an impulse occurs with a weighting given by  $a_i$ . The primary process points are not weighted.

The first assumption is supported by the periodicity in the data that is related to the fundamental frequency of the power line. The large majority of observed gap-noise sources had pulse groups on both the positive and negative phases of the fundamental waveform, and accounts for the  $T_0/2$  periodicity.

The second assumption addresses the differences between

the sparking phenomena on the positive and negative phases of the fundamental waveform. It is commonly observed that the  $E[N_{\text{pos}}]$  is slightly different from  $E[N_{\text{neg}}]$ , where  $N_{\text{pos}}$  and  $N_{\text{neg}}$  are the random number of discharges in a pulse group. This difference can be due to two effects: an asymmetrical gap geometry and the fundamental physical difference between the sparking mechanisms for positive-to-ground and negative-to-ground sparks. A deterministic integer constant  $N$  nearest to  $\{E[N_{\text{pos}}] + E[N_{\text{neg}}]\}/2$  is assumed as the approximation to the variable number of sparks per half-cycle of the fundamental waveform.

The third assumption is based on the fact that the ‘‘inception of gap discharges in natural air and the development of electron avalanche are fundamentally probabilistic processes that depend on atmospheric pressure, humidity, presence of natural ions, electrode surface and so on’’ [13]. In view of the above statement and considering the empirical data, the justification for developing the gap discharge as a random process is well founded. The assumption of independence from discharge to discharge is not as well justified. Effects such as electrode heating after the initial discharge in a cycle could act to make the average interarrival time vary from pulse to pulse within a pulse group. However, to develop a tractable model, the assumption of independence between arrival times was made. The gamma density function determined by the estimate of the mean and variance of the interarrival times is used to define the probability density function of the interarrival times.

The fourth assumption concerns the amplitude of the impulses. In most cases, the amplitude of the impulses within a pulse was nearly constant. In some cases, there was a difference in the average amplitude from negative phase to positive phase; however, being consistent with the other assumptions, the average value was determined by averaging over both phases. The estimate of the mean of the impulses defines the constant  $a$ .

The above assumptions place this model in a class of processes known as branching processes with the primary process being an equilibrium renewal process with an interarrival probability density function of

$$f(t) = \delta(t - T_0/2) \quad (9)$$

and the subsidiary process being an ordinary renewal process with a gamma interarrival probability density function.

Summarizing, the gap-noise model is specified by the following parameters:

$a$	amplitude of impulses,
$N$	number of impulses in subsidiary process,
$\bar{\mu}$	mean value of impulse interarrival time,
$\sigma_\mu$	variance of impulse interarrival time, and
$N_0B/2$	Gaussian noise power in the in-phase and quadrature channels.

A sample realization of the noise process defined above, over an interval  $T$ , is given by

$$n(t) = g(t) + \sum_{m=1}^{M(T)} \sum_{n=1}^N a e^{j\theta_{mn}} h(t - t_{mn} - mT_0/2) \quad (10)$$

where  $M(T)$  is the number of half power-line periods  $T_0/2$  in the observation interval  $T$ . Fig. 7 shows a realization of the envelope of this process for  $N = 3$ ,  $T = 30$  ms and gamma density function parameters  $r = 32$  and  $\lambda = 37\,000$ . The method presented in [14] was used to generate random interarrival times with a gamma density. The impulse amplitudes were normalized to one and a background level of quadrature Gaussian noise at  $N_0B/2 = 0.0001$  was added, which simulates either receiver noise or high-density low-amplitude impulsive noise. Note that, in comparison to an actual noise process illustrated in Fig. 3, there is a fixed number of impulses on the positive and negative polarity of the line voltage waveform. This is a consequence of the simplifying assumptions.

## V. COMPARISON OF CALCULATED AND OBSERVED SPECTRUM

One partial description of a noise process is the amplitude probability distribution of the envelope. This descriptor has been used extensively in the analysis of noise and deriving optimum receivers. For the  $N(t)$  that has been specified in the model presented above, this calculation would be very difficult. A second noise process descriptor is the spectrum of the noise process. This descriptor is suited to our model where the structure of the noise is contained in the counting process that drives the impulse generation. In addition to receiver noise performance evaluation, spectral analysis can also be used for noise-source identification and isolation.

As a test of the model, the power spectral density (PSD) of the envelope of the gap-noise process shown in Fig. 4 was determined using a spectrum analyzer and also analytically determined using only the model parameters from the time-domain data. With (10) as a starting point, it is shown in the Appendix that the average of a Bartlett estimate of the PSD of the envelope of the impulsive component of the noise is given by

$$\begin{aligned} \bar{S}(\omega, T) = & a^4 T^{-1} |H_2(\omega)|^2 \\ & \cdot \left\{ \left[ \frac{\cos(M\pi\omega/\omega_0) - 1}{\cos(\pi\omega/\omega_0) - 1} - M \right] \theta(\omega, N) \right. \\ & \left. + M\Phi(\omega, N) \right\} \end{aligned} \quad (11a)$$

where

$$H_2(\omega) = F[|h(t)|^2] \quad (11b)$$

$$\theta(\omega, N) = \frac{|\phi(j\omega) - \phi(j\omega)^{N+1}|^2}{|1 - \phi(j\omega)|^2} \quad (11c)$$

$$\Phi(\omega, N) = \frac{N - N|\phi(j\omega)|^2}{|1 - \phi(j\omega)|^2} - 2 \operatorname{Re} \left\{ \frac{\phi(j\omega)(1 - \phi(j\omega)^N)}{(1 - \phi(j\omega))^2} \right\} \quad (11d)$$

and  $\phi(j\omega)$  is the characteristic function of the gap-noise pulse spacing (first interarrival time). For large  $N$ , the first term of  $\Phi(\omega)$  dominates. Equation (11a) clearly shows the effects on the PSD of the envelope of the filter  $H_2(\omega)$ , the power-line frequency, and the interarrival time spacing of the individual



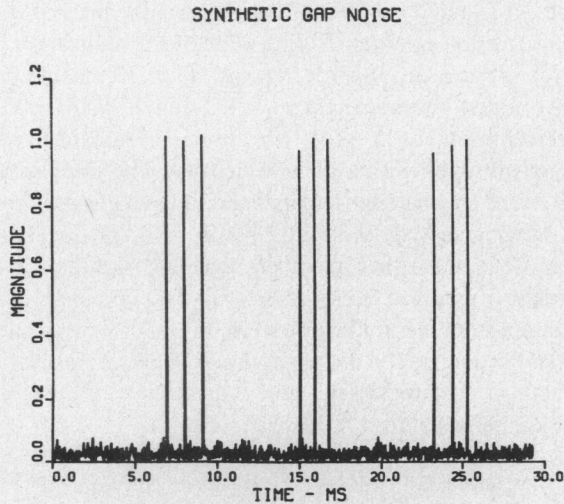


Fig. 7. Envelope of synthetically generated gap noise with parameters  $N = 3$ ,  $N_0B/2 = 0.0001$ ,  $a = 1$ ,  $\mu = .83$  ms, and  $\sigma_\mu = 2.3 \times 10^{-6}$  ms<sup>2</sup>.

impulses. The first term in (11a) is due to the intrapulse correlations and consists of an envelope times a comb function. The second term in (11a) is continuous spectra due to the correlations within a pulse group.

Fig. 8 is a computer plot of the analytic estimate of the PSD which is compared with the observed PSD computed on a Wavetek UA500A spectrum analyzer shown in Fig. 9. Comparing the two PSD's, it is seen that the analytical expression correctly predicts the significant features seen in the observed PSD. The 120-Hz spacing of the peaks in the PSD is due to the fundamental ac waveform and the envelope of the 120-Hz peaks is due to the correlations between the intrapulse interarrival times. The continuous spectra, which appear as a colored noise floor, peak at 1100 Hz in both spectra and are due to the interpulse correlations. The main difference between the actual and predicted PSD is the presence in the actual PSD of 60-Hz harmonics and the changeover at 1000 Hz of the predominate peaks from 120-Hz harmonics to odd 60-Hz harmonics. This is due to the previously discussed possible differences between the positive and negative phases of the impulse groups in amplitude, average number of pulses per group, and interarrival distribution.

## VI. CONCLUSION

A five-parameter model for a single source of gap-noise disturbance has been developed and shown to predict the major features of the PSD of a narrow-bandwidth demodulated gap-noise source. The model is less accurate in predicting the exact amplitudes of the frequency components.

Further research is needed to define the range of values of the above parameters, to determine the effects construction practices and weather have on parameters, and to examine the susceptibility of various types of communications equipment to simulated gap-noise within the range of likely parameters.

It has been stated that, in engineering design, one seeks not so much to be optimum but to avoid crippling nonoptimalities [15]. It is intended that this research will permit system designers to subject their systems to simulated disturbance

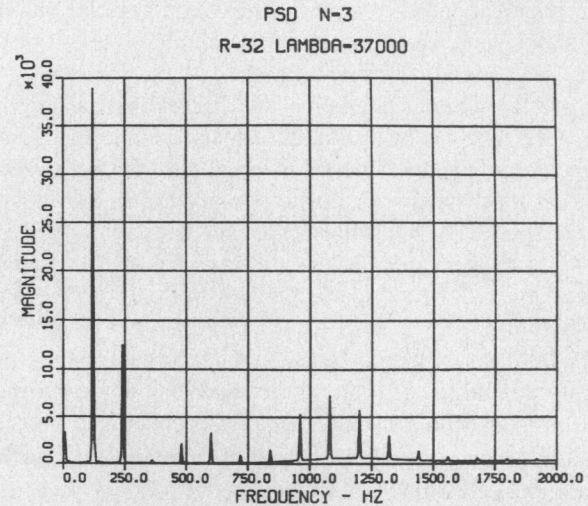


Fig. 8. Predicted Bartlett estimate of PSD of gap-noise envelope using model parameters. Same process as shown in Fig. 4.

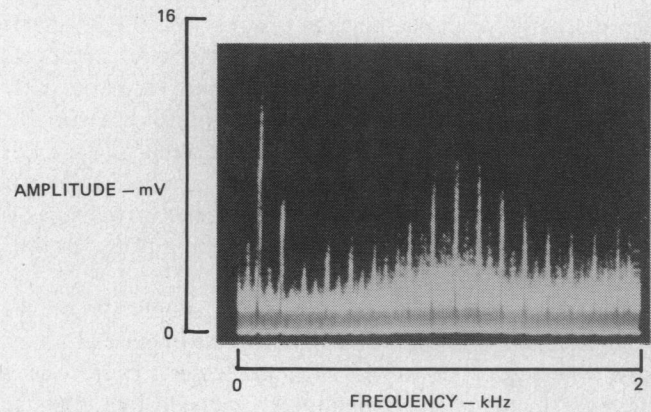


Fig. 9. Observed Bartlett estimate of PSD of gap-noise envelope measured using Wavetek UA500A and 3-D display. Same process as shown in Fig. 4.

based on the model presented. The robustness of the system in an actual gap-noise environment can then be evaluated. This research should be particularly applicable to systems that operate from a fixed site, within line of sight of power lines where the chances of having a major gap-noise disturbance source are significant.

## APPENDIX

The complex envelope representation of filtered impulse noise arising from a branching renewal process on a finite interval  $T$  is given by

$$n(t) = \sum_{m=1}^{M(T)} \sum_{n=1}^{N_m} a_{mn} e^{j\theta_{mn}} h(t - t_{mn} - T_m) \quad (12)$$

where  $T_m$  is the beginning of the  $m$ th main interval,  $N_m$  is the number of impulses in the  $m$ th interval, arriving at times  $\{t_{mn}\}$  after its onset, and  $M(T)$  is the number of main events in the observation interval  $T$ . The pulse amplitudes  $\{a_{mn}\}$  and phases  $\{\theta_{mn}\}$  are statistically independent random variables and the  $\{t_{mn}\}$  are taken to be uniform on  $\{0, 2\pi\}$ . The net filtering effects on the impulses are accounted for by the time-invariant complex-envelope impulse response  $h(t)$ .

We seek the PSD of the squared envelope

$$E^2(t) = n(t)n^*(t) = \sum_{m=1}^{M(T)} \sum_{n=1}^{N_m} a_{mn}^2 |h(t - t_{mn} + T_m)|^2 \quad (13)$$

where we have neglected terms of the form  $h(t - t_{mn} - T_m)h^*(t - t_{lk} - T_m)$  for  $lk \neq mn$  by assuming  $h(t)$  is sufficiently short, and the impulses sufficiently sparse so that there is an insignificant chance of pulse overlap. An estimate of the PSD of the envelope may be obtained by averaging successive magnitude squared, length  $T$ , Fourier transforms of  $E^2(t)$ . This is known as a Bartlett estimate. The mean value of the estimate is

$$\bar{S}(\omega, T) = E[|\epsilon_2(\omega, T)|^2]/T \quad (14)$$

where  $\epsilon_2(\omega, T)$  is the length  $T$  Fourier transform of  $E^2(t)$ . Specifically,

$$\epsilon_2(\omega, T) = \sum_{m=1}^{M(T)} \sum_{n=1}^{N_m} a_{mn}^2 e^{-j\omega t_{mn}} e^{-j\omega T_m} H_2(\omega) \quad (15)$$

with  $H_2(\omega) = \int_0^T |h(t)|^2 e^{-j\omega t} dt$ , the Fourier transform of the magnitude-squared impulse response. To find the mean of the estimate, we must evaluate

$$\bar{S}(\omega, T) = E \left[ |H_2(\omega)|^2 \sum_{m=1}^{M(T)} \sum_{n=1}^{N_m} \sum_{l=1}^{M(T)} \sum_{k=1}^{N_l} a_{nm}^2 a_{lk}^2 \cdot e^{-j\omega(t_{mn} - t_{lk})} e^{-j\omega(T_m - T_l)} \right] / T. \quad (16)$$

In order to simplify this expression, we make the following restrictions:  $E(a_{mn}^2 a_{lk}^2) = a^4$ , a constant, and  $N_m = N_l = N$ , a constant, and  $f(t_{mn}) = f(t_{ln})$ ; that is, the arrival times in each of the main process intervals are identically distributed. Furthermore, let  $M$  main process points occur at intervals  $T_0/2$  of a fundamental frequency (in our case  $f_0 = \omega_0/2\pi = 1/T_0 = 60$  Hz, the power-line frequency). Then (16) becomes

$$\bar{S}(\omega, T) = a^4 |H_2(\omega)|^2 \left[ \sum_{m=1}^M \sum_{l=1}^M e^{-j\omega(m-l)T_0/2} \right] \cdot \sum_{n=1}^N \sum_{k=1}^N E[e^{-j\omega(t_{mn} - t_{lk})}] / T. \quad (17)$$

The remaining random quantity,  $E[e^{-j\omega(t_{mn} - t_{lk})}]$  must now be evaluated for two distinct cases. These are: 1) where  $m = l$ , which are the summations over the intrapulse group terms; and 2)  $m \neq l$ , which are the summations over the interpulse group terms. Now, rearranging the summations,

$$\bar{S}(\omega, T) = a^4 |H_2(\omega)|^2 \left\{ \left[ \sum_{v=0}^{M-1} \sum_{\substack{u=-v \\ u \neq 0}}^v (e^{-j\pi\omega/\omega_0})^u \right] \cdot \left[ \sum_{n=1}^N \sum_{k=1}^N E(e^{-j\omega t_n}) E(e^{j\omega t_k}) \right] \right\}$$

$$+ M \left[ \sum_{k=0}^{N-1} \sum_{i=-k}^k E(e^{-j\omega t_i}) \right] \Bigg\} / T \quad (18)$$

where  $t_i = t_n - t_k$  is the  $i$ th subsidiary process interarrival time. Since the pulse arrivals are statistically independent

$$E(e^{-j\omega t_i}) = \begin{cases} \phi^i(j\omega), & t_i \geq 0 \\ \phi^i(-j\omega), & t_i < 0 \end{cases} \quad (19)$$

where  $\phi(j\omega)$  is the characteristic function of the pulse spacing (first interarrival time). Evaluating the finite sums, one obtains

$$\bar{S}(\omega, T) = a^4 T^{-1} |H_2(\omega)|^2 \left\{ \left[ \frac{\cos(M\pi\omega/\omega_0) - 1}{\cos(\pi\omega/\omega_0) - 1} - M \right] \theta(\omega, N) + M\Phi(\omega, N) \right\} \quad (20a)$$

where

$$\phi(\omega, N) = \frac{|\phi(j\omega) - \phi(j\omega)^{N+1}|^2}{|1 - \phi(j\omega)|^2} \quad (20b)$$

and

$$\Phi(\omega, N) = \frac{N - N|\phi(j\omega)|^2}{|1 - \phi(j\omega)|^2} - 2 \operatorname{Re} \left\{ \frac{\phi(j\omega)(1 - \phi(j\omega)^N)}{(1 - \phi(j\omega))^2} \right\}. \quad (20c)$$

As  $N$  goes to infinity, the first term of  $\Phi(\omega, N)$  dominates and is a general expression for the spectrum of a renewal process in terms of the characteristic function of the interarrival times [16].

#### ACKNOWLEDGMENT

The authors would like to acknowledge gratefully the assistance given to them by Prof. S. Jauregui and Prof. W. R. Vincent of the Naval Postgraduate School. Prof. Jauregui sponsored the research and reviewed the results, and Prof. Vincent developed the instrumentation used to collect the data and freely provided his expertise in gathering and interpreting the data.

#### REFERENCES

- [1] E. J. Cummins, S. Jauregui, and W. R. Vincent, "Time- and frequency-domain characteristics of man-made radio noise affecting HF-communications sites," *IEEE Trans. Electromagn. Compat.*, vol. EMC-21, no. 3, pp. 182-189, Aug. 1979.
- [2] J. R. Herman, "Survey of man-made radio noise," in *Progress in Radio Science*. Brussels, Belgium: Int. Union Radio Scientists, 1970, pp. 315-408.
- [3] D. Middleton, "Statistical-physical models of electromagnetic interference," *IEEE Trans. Electromagn. Compat.*, vol. EMC-19, no. 3, pp. 106-127, Aug. 1977.
- [4] W. E. Pakala and V. L. Chartier, "Radio wave measurements on overhead power lines from 2.5 to 800 kV," *IEEE Trans. Power App. Syst.*, vol. PAS-90, no. 3, p. 1155, May/June 1971.
- [5] E. N. Skomal, *Man-made Radio Noise*. New York: Van Nostrand Reinhold, 1978, p. 83.
- [6] P. A. W. Lewis, "Asymptotic properties of branching renewal processes," IBM, Tech. Rep. RC-2878, pp. 2-5, May 1970.

- [7] D. R. Cox, *Renewal Theory*. London, England: Methuen, 1962, p. 18.
  - [8] H. J. Larson, *Introduction to Probability Theory and Statistical Inference*. New York: Wiley, 1974, p. 250.
  - [9] J. W. Modestino, K. Y. Jung, and K. R. Matis, "Modeling, analysis and simulation of receiver performance in impulsive noise," in *GLOBECOM '83 Conf. Rec.*, 1983, pp. 1598-1605.
  - [10] T. Kailath, "The complex envelope of white noise," *IEEE Trans. Inform. Theory*, vol. IT-12, no. 3, pp. 397-398, July 1966.
  - [11] J. V. DiFranco and W. L. Rubin, *Radar Detection*. New York: Prentice-Hall, 1968, p. 299.
  - [12] P. Beckmann, "Amplitude probability distribution of atmospheric radio noise," *Radio Sci.*, vol. 68D, pp. 726-727, June 1964.
  - [13] K. Arai, W. Janischewskyj, and N. Miguchi, "Micro-gap discharge phenomena and television interference," *IEEE Trans. Power App. Syst.*, vol. PAS-104, no. 1, pp. 224-224, Jan. 1985.
  - [14] M. Abramowitz and I. Stegun, *Handbook of Mathematical Functions*. Washington, DC: GPO, 1964, p. 951.
  - [15] J. M. Wozencraft and I. R. Jacobs, *Principles of Communication Engineering*. New York: Wiley, 1965, p. 459.
  - [16] D. R. Cox and H. D. Miller, *The Theory of Stochastic Processes*. New York: Wiley, 1965, p. 359.
-